
STOCHASTIC FIRST-ORDER LEARNING FOR LARGE-SCALE FLEXIBLY TIED GAUSSIAN MIXTURE MODEL

Mohammad Pasande, Reshad Hosseini, Babak N. Araabi

School of ECE

College of Engineering

University of Tehran, Tehran, Iran

{mohammad.pasande, reshad.hosseini, araabi}@ut.ac.ir

ABSTRACT

Gaussian Mixture Models (GMM) are one of the most potent parametric density estimators based on the kernel model that finds application in many scientific domains. In recent years, with the dramatic enlargement of data sources, typical machine learning algorithms, e.g. Expectation Maximization (EM), encounters difficulty with high-dimensional and streaming data. Moreover, complicated densities often demand a large number of Gaussian components. This paper proposes a fast online parameter estimation algorithm for GMM by using first-order stochastic optimization. This approach provides a framework to cope with the challenges of GMM when faced with high-dimensional streaming data and complex densities by leveraging the flexibly-tied factorization of the covariance matrix. A new stochastic Manifold optimization algorithm that preserves the orthogonality is introduced and used along with the well-known Euclidean space numerical optimization. Numerous empirical results on both synthetic and real datasets justify the effectiveness of our proposed stochastic method over EM-based methods in the sense of better-converged maximum for likelihood function, fewer number of needed epochs for convergence, and less time consumption per epoch.

Keywords GMM · First-Order Optimization, Stochastic Optimization · Manifold Optimization

1 Introduction

Gaussian Mixture Models (GMMs) are one of the most famous Kernel Models used in a vast set of problems [1]. Image representation[2], robot movements learning[3], improving deep learning by expanding batch normalization[4], latent variable modeling [5], and even performing as generative models [6] are some of the applications of Gaussian Mixture Models.

In a nutshell, there are three prominent families of approaches to deal with parameter estimation of GMMs, a) well-known Expectation Maximization (EM)[7], b) Mixture Density Networks[8], and c) Numerical Optimization[9]. The EM and its extensions[10] are still more favorable to the community. Each variation has tried to cover some regions; for instance, to broaden the batch regime's horizon, an incremental adaption of it has been introduced[11], or recently, a hybrid maximization algorithm (Coordinate Descent - Fast Newton Minimum Residual EM) has achieved a very fast convergence in many practical examples[12]. Unlike the EM-based method, numerical optimization approaches have not been fortunate due to two main reasons; firstly, the likelihood maximization can be interpreted as KL-divergence minimization, which does not provide a sufficient sense of distance in far ranges from optimal point[5, 13]. Secondly, nonconvex optimization with the implicit Positive Definiteness (PD) constraint on the covariance matrix is challenging. Even though it has been shown that an Interior Point algorithm can handle a PD constraint through a group of smooth convex inequalities [14], with a high dimensional problem, such a method faces slow convergence in comparison with EM-based algorithms.

With the difficulties of numerical optimization mentioned, In[15] the problem was attacked by leveraging Manifold Optimization in a combination of a "reformulation trick" to employ sophisticated algorithms such as L-BFGS and Conjugate Gradient. Furthermore, In [16] authors has shown that Riemannian Stochastic Gradient Descent

outperforms other existing methods (i.e. The success key of RSGD in this setup was due to the reformulation trick and conducting the algorithm along the manifold of positive definite matrices, it performed as a Natural Gradient Descent[17].) Despite the fact that recent manifold-powered algorithms remedies the bias error caused by spherical covariance matrices structure of GMMs and be able to expand to high-dimensional problems, the full covariance matrices plea expensive computation as well, which may not be suitable in case of demanding a large number of components.

Our contributions and motivations for the investigation come in three parts:

- First to propose using a framework of structural modification[18] with similarities to eigenvalue-vector decomposition but containing computation obligation named flexibly-tied covariance then as in a numerical optimization fashioned problem, and the Negative LogLikelihood minimized with a first-order online method. Also, to avoid confronting singularity in parameter estimation[19], a common approach of penalizing the LogLikelihood is suggested[20].
- Second, as was shown in prior work [12], the orthogonal constraint on eigenvalue-vector factorization[21] estimation performed inferior to free-style structure and also was very restricted to engage with high-dimensional with a large number of components. Thus, an online first-order optimization framework preserving orthogonality constraint was introduced to lift the burden of mentioned tribulations.
- Third, a favorable side product of using orthogonality constraint is the elimination of determinate computation in any following procedure. However, with the suggestion of [22], the PLU factorization would be used to achieve an unconstrained optimization procedure with low-cost determinant computation.

From this point forward, in section 2, we formulate GMM with large-scale consideration, and structural modification can be done; additionally, stochastic first-order gradient-based optimization of nonconvex objective functions is presented in the same section. Moreover, a geometrical point of view of orthogonality constraint is discussed in the sense of Manifold Optimization in section 3, and a new stochastic orthogonality preserving optimizer is introduced. Experiments, including an empirical investigation of the performance of mentioned methods, is illustrated in section 4 alongside experiments on real data. Finally, we conclude our paper with section 5.

2 Flexibly Tied Gaussian Mixture Model

The GMM density for $x \in \mathbb{R}^N$ is as follows

$$p(x) = \sum_{k=1}^K \pi_k \mathcal{N}(x; \mu_k, \Sigma_k^{-1}) \quad (1)$$

$$\text{Where } \mathcal{N}(x; \mu_k, \Sigma_k^{-1}) = (2\pi)^{-N/2} \det(\Sigma_k)^{-1/2} \exp\left(-\frac{1}{2}(x - \mu_k)^T \Sigma_k^{-1} (x - \mu_k)\right).$$

Therefore, the explicit constraint optimization by consideration of n i.i.d. samples as $\{x_1, x_2, \dots, x_n\}$ arises here as minimizing the Negative Log-Likelihood (NLL)

$$\begin{aligned} & \underset{\pi_k, \mu_k, \Sigma_k}{\text{minimize}} && - \sum_{i=1}^n \log \left\{ \sum_{k=1}^K \pi_k \mathcal{N}(x_i; \mu_k, \Sigma_k^{-1}) \right\} \\ & \text{subject to} && \sum_{k=1}^K \pi_k = 1 \ \& \ \pi_k \geq 0. \\ & && \Sigma_k^{-1} \succeq 0 \quad \forall k. \end{aligned} \quad (2)$$

The optimization approach for covariance matrices is dependent on their structure. Covariance structure regards two entities, dependency and shape. The first entity allows how many components are able to have their own covariance, and the second discusses the form of the estimated matrices. This results in two extremes on the covariance structure; on the one hand, diagonal covariance, which, because of the cheap computation, allows each component to have its covariance; on the other hand, full covariance, which has more capability to grasp the properties of data. The full covariance raises concerns about positive definiteness constraints; hence [23] suggested to use of Cholesky factorization. However, in practice, for the expensive computation, the covariance shape has to be fixed for a large number of

components.

The flexibly-tied factorization is suggested [18, 12], To have the best of both worlds (flexibility and low computation)

$$\Sigma_k^{-1} = U D_k U^T \quad (3)$$

Where U is the shared parameter between all components, and D_k is a component-wise diagonal matrix; Table 1 illustrates the characteristics of each model by the factors of the number of parameters and type of employed algorithm.

Table 1: Characteristics of Covariance shapes [24]		
Cov. Shape	No. Parameter	M-step
Diagonal	$K(N)$	Closed Form
Full	$K \frac{N(N+1)}{2}$	Iterative Algorithm
Flexibly-Tied	$K(N) + (N)^2$	Iterative Algorithm

As a result of the quadratic form of this factorization, the PD constraint is restricted to the positiveness of diagonal elements of the D_k , which can be satisfied by using a SoftPlus function.

$$\forall j = \{1, 2, \dots, N\} \quad d_k^{(j)} = \frac{1}{\beta} \log(1 + \exp(\beta \tilde{d}_k^{(j)})) \Rightarrow \Sigma_k^{-1} \succeq 0 \quad (4)$$

Moreover, to handle the Convex combination of K components constraint, a mediating variable α_k can replace the original π_k , and by a nonlinear function (SoftMax) leads to the desired solution[25, 15].

$$\alpha_k = \log\left(\frac{\pi_k}{\pi_K}\right) \quad \text{or} \quad \pi_k = \frac{\exp(\alpha_k)}{\sum_{k=1}^K \exp(\alpha_k)} \Rightarrow \sum_{k=1}^K \pi_k = 1 \ \& \ \pi_k \geq 0 \quad (5)$$

2.1 Penalized Cost Function

The singularity of the parameter estimation result may appear in two different aspects, first as in the weights of components, in which one component probability grows almost to one, and second the singularity of the covariance matrix itself. We penalize the LogLikelihood function with a combination of multivariable Gaussian distribution's conjugate prior and symmetric Dirichlet. Hence, we have three parts for the penalizing term as follows

- The Wishart prior on U , with the degree of freedom of $n + 2$ and S as scale matrix

$$\psi_1(UU^T) = \frac{1}{2} \log(\det(UU^T)) - \frac{1}{2} \text{tr}(UU^T S^{-1}) + \text{Const}_1 \quad (6)$$

Where S is $\frac{1}{K} \frac{1}{n} \text{Cov}(X)$. For the D_k , the Gamma distribution is defined as the penalizer

$$\psi_2(D) = \sum_{k=1}^K \sum_{i=1}^N -\frac{s}{2} d_{ki} + \frac{N}{2} \log(d_{ki}) + \text{Const}_2 \quad (7)$$

Where s is $\frac{1}{N} \frac{1}{K} \sum_k \text{diag}(\text{Cov}(X))$.

- With the assumption of a given covariance matrix Σ^{-1} in a multivariate Gaussian, a Multivariate Gaussian distribution is the conjugate prior recommended; thus, we have

$$\psi_3(\mu) = \sum_{k=1}^K -\frac{1}{2} (\mu_k - \mu_p)^T \Sigma_k^{-1} (\mu_k - \mu_p) - \frac{1}{2} \log(\det(\frac{K}{2\pi} \Sigma_k^{-1})) \quad (8)$$

Where the μ_p is the empirical mean of data, and the K is the shrinkage variable set to 0.01.

- Symmetric Dirichlet distribution is considered the prior for the component's weights, and thus, with equation5, we have the penalizer as follows

$$\varphi(\alpha) = \zeta \sum_{k=1}^K \alpha_k - K \zeta \log\left(\sum_{k=1}^K \exp(\alpha_k)\right) \quad (9)$$

Where the ζ is the concentration parameter.

2.2 Estimation

With all the preparation and considerations, we can proceed to rewrite the minimization problem in equation 2 as an unconstrained problem as below

$$\underset{\alpha_k, \mu_k, U, D_k}{\text{minimize}} - \sum_{i=1}^n \log \left\{ \sum_{k=1}^K \frac{\exp(\alpha_k)}{\sum_{k=1}^K \exp(\alpha_k)} \mathcal{N}(x_i; \mu_k, U, D_k) \right\} + \psi(U, D, \mu) + \varphi(\alpha) \quad (10)$$

where $\psi(U, D, \mu)$ is the weighted combination of equations 6, 7, and 8 showed in equation 11, also for the sake of convenience, a weight scalar were assigned to each. Additionally, the $\varphi(\alpha)$ is defined in equation 9 with ζ acting as a weight.

$$\psi(U, D, \mu) = w_1 \psi_1(UU^T) + w_2 \psi_2(D) + w_3 \psi_3(\mu) \quad (11)$$

The optimization procedure is straightforward by the formulation in equation 10 and, as a sample, by the illustrated results in section 4, the estimation procedures do not face singularity difficulties without any posterior estimation in the majority of cases. Furthermore, One way to handle the estimation problem is to use a First-Order Stochastic optimizer such as stochastic gradient descent (SGD.) Moreover, in actual practice, we can use a modified version of SGD such as SGD with momentum, adaptive estimate like ADAM [26], or Clipping SGD [27]. While this approach is easy to implement, the covariance determinant computation can be reduced.

To follow this motivation, In [22], the authors introduced a PLU factorization of a matrix where L is a down triangular matrix with the diagonal element of one, \tilde{U} is an upper triangular matrix with the diagonal element of zero, and s is a vector with the motivation of reducing determinant computation. Estimating the U parameter via this factorization provides the opportunity for computation reduction like in equation 12.

$$U = L(\tilde{U} + \text{diagonal}(s)) \Rightarrow \det(\Sigma_k^{-1}) = \prod_i s_i^2 d_{i,i} \quad (12)$$

Although the PLU remedies the computation cost, another technique based on the properties of the Felexiby-Tied may be discussed. Prior to this work, In [24], the authors investigated all eigenvalue-vector factorization for covariance matrices, while, in [12], it is illustrated that the orthogonality constraint faces several difficulties in the case of high-dimensional data and a large number of components. In contrast, we suggest using a stochastic manifold-based version of optimizers. Furthermore, within the next section, we cover the basic requirements for using the Riemannian manifold in our favor and introduce a new manifold stochastic gradient-based algorithm.

The Orthogonality constraint that is enforced to our covariance factorization reduced the determinant computation to a multiplication of diagonal elements of matrix D in each component. In addition, to increase the flexibility of our model, a component-wise scaler variable is added to our covariance factorization which is written as equation 13.

$$\Sigma_k^{-1} = \lambda_k U D_k U^T \Rightarrow \det(\Sigma_k^{-1}) = \lambda_k \prod_i d_{i,i} \quad (13)$$

3 Proposed Orthogonality Preserving Algorithm

3.1 Manifold Optimization

Smooth Manifolds " \mathcal{M} " are spaces with smooth transitions between subsets that are locally Euclidean-like. The *Tangent Space* to a smooth Manifold " $T_x \mathcal{M}$ " is the set containing all the linearized representations of all curves passing a given point on the manifold; this space locally acts as a vector space. The *Riemannian manifold* " (\mathcal{M}, g) " is a smooth Manifold which is equipped with a *Riemannian metric* " $g(\zeta_x, \xi_x) = \langle \zeta_x, \xi_x \rangle_x$," a Riemannian manifold is a particular structure allowing the calculus needed to establish optimization algorithms. Riemannian manifold leverage the fact that manifold-aware unconstrained optimization on certain condition can be seen as an Euclidean constrained optimization problem. Thus, to use this tool to our advantage, several important properties of the manifolds are addressed in the sequel. Details can be found in [28] and [29].

Geodesic is the shortest smooth curve connecting two fixed points on a manifold. An *Exponential map* " $Exp_x(\cdot)$ " represents a geodesic that maps a vector in the tangent space to the manifold $\gamma(t) : t \in [0, 1]$; due to the expensive computation of using an exponential map, a *Retraction* is preferred " $\mathcal{R}_x : T_x \mathcal{M} \rightarrow \mathcal{M}$ ", which is a more general operator with exact first-order approximation like the exponential map Figure 1. *Parallel Transport* is introduced to handle carrying vectors along a geodesic, allowing the ability to move isometrically. However, *Vector Transport* is a smooth mapping on manifold associated with a specific retraction function which replaces Parallel Transport in practice due to computation efficiency. " $w_x \in T_x \mathcal{M}$ and $\tau : T_x \mathcal{M} \times T_x \mathcal{M} \rightarrow T_{\mathcal{R}(w_x)} \mathcal{M}$ "

3.2 Orthogonality Constraint

The Stiefel manifold is defined as p orthogonal columns in n -dimensional space, $St(n, p) = \{X \in \mathbb{R}^{n \times p} : X^T X = I_p\}$. There are two extreme versions of this matrix manifold, first $p = 1$, which create the Sphere in Euclidian space, $S^{d-1} = \{X \in \mathcal{E} (d = \dim(\mathcal{E})) : \|x\| = 1\}$; the second version is $p = n$ that shapes the Special Orthogonal Groups : $\mathcal{O}(n) = \{X \in \mathbb{R}^{n \times n} : X^T X = I_n\} \rightarrow \mathcal{SO}(n) = \{X \in \mathcal{O}(n) : \det(X) = +1\}$.

Some preliminaries are needed to work with the Special Orthogonal Groups; the Tangent space is the Skew-Symmetric Matrices which holds the property of vector calculus, and the Riemannian metric is the same as Euclidean metric since we consider $\mathcal{SO}(n)$ as an embedded submanifold of Euclidean space. Projection onto the tangent space can be obtained by a simple product $Proj_X U = AX$; in which the A represents an auxiliary skew-symmetric matrix as follow

$$A \triangleq 2 \times Skew(UX^T) \quad \text{or} \quad A \triangleq 2 \times Skew\left(\left[I - \frac{1}{2}XX^T\right]UX^T\right) \quad (14)$$

where in equation 14 the "Skew" function is a typical skew-symmetric form of any matrices, $Skew(Y) = \frac{1}{2}(Y - Y^T)$. The choice of retraction function is between various options, but the most famous ones can be summarized as follow: a) QR factorization, b) Polar decomposition (using SVD decomposition) [28], c) Cayley transform [30]. At last, the vector transport due to the geometry of the problem can be achieved by multiplication of an identity matrix.

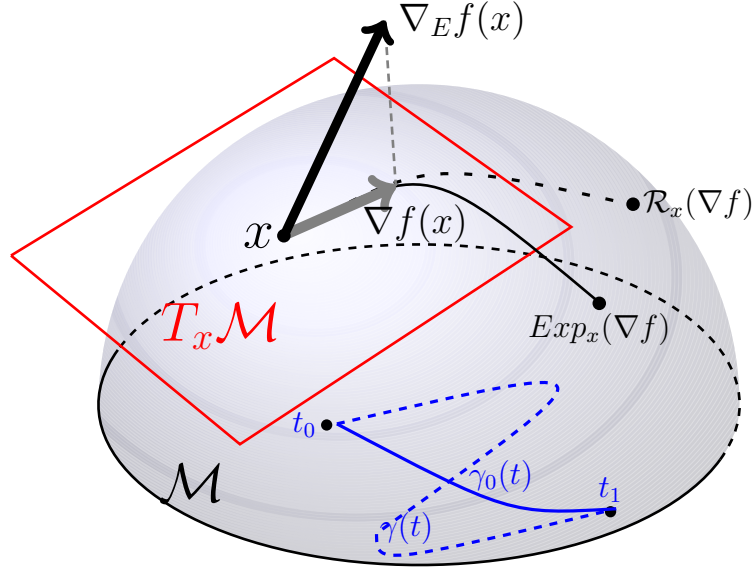


Figure 1: A typical example of a manifold is the sphere, an n -dimensional manifold embedded in $(n + 1)$ -dimensional space, $\{x \in \mathbb{R}^{n+1} \mid \|x\|_2 = 1\}$. At any given x , there is a corresponding tangent space (an n -dimensional vector space that can illustrate the Riemannian metric as $g : T_x \mathcal{M} \times T_x \mathcal{M} \rightarrow \mathbb{R}$). The blue dashed line $\gamma(t)$ is a smooth curve on the manifold between two nominal points, and the solid curve is so-called geodesic $\gamma_0(t)$. Note that the $\nabla_E f$ and ∇f indicate the Euclidean gradient and Riemannian gradient at point x , respectively. The solid black line $Exp_x(\cdot)$ shows the geodesic curve along the Riemannian gradient vector on the manifold itself, better known as the exponential map. Therefore, the loosely black dashed line $\mathcal{R}_x(\cdot)$ is its compute efficient alternative (Retraction function).

3.3 Stochastic Optimization

The formulated optimization problem can be presented in many applications as a Finite Sum Problem 15.

$$\min_{X \in \mathcal{M}} f(x) \triangleq \frac{1}{n} \sum_{i=1}^n f_i(x) \quad (15)$$

Due to the scheme of the problem, which is usually large-scale (in the sense of data points and scalability of the model itself), the first-order methods suffer from expensive gradient computation; thus, a stochastic/incremental approach is recommended, such as (SGD). On the other hand, Riemannian stochastic methods follow the same pattern as their Euclidean counterparts; they substitute the descent direction with an approximation of it.

$$x_{t+1} \leftarrow \mathcal{R}_{x_t}(-\eta_t \nabla f_{i_t}(x_t)) \quad (16)$$

Without loss of generality, the Reimmanian SGD [31] is presented as equation 16 at each iteration t where i_t comes from a discrete uniform distribution. In addition, the α_t is a learning rate (stepsize) typically satisfies $\sum_t \eta_t = \infty$ and $\sum_t \eta_t^2 \leq \infty$.

3.4 Reimmanian Stochastic Gradient Clipping

It is a common assumption to believe the objective function landscape holds an L-smoothness property. The definition of the L-smooth function in embedding space comes as follows

Definition 1 (L-Smoothness). f is L-Smooth, if there exist positive constants L s.t. $\forall x, y \in \mathbb{R}^n$ in embedding space

$$f(y) \leq f(x) + \langle \nabla_E f(x), y - x \rangle + \frac{L}{2} \|y - x\|^2. \quad (17)$$

Assumption 1. *The nonconvex objective function is L-Smooth in the embedding space..*

The *Clip* procedure usually includes two significant types Global Clipping "*GClip*" and Coordinate-wise Clipping "*CClip*"; the *GClip* implies magnitude modifications only with the central assumption of the resemblance of noise in every coordination is the same [27], therefore, in this paper, the focus is dedicated to *CClip* owed to the flexibility it provides through every coordination.

The Assumption 3.4 allows us to benefit from the goodness of the coordinate-wise scheme in embedded space.

Assumption 2. $\nabla f_j(x)_i$ is the stochastic coordinate-wise Mani gradients for $i \in \{1, 2, \dots, N\}$. There exist constants $B_i \geq 0$ and $\theta \in (1, 2]$ s.t. $\mathbb{E}[|\nabla f_j(x)_i|^\theta] \leq B_i^\theta$.

At last, The general stochastic gradient descent with clipping procedure on $\mathcal{SO}(n)$ is illustrated in Algorithm 1.

Algorithm 1 Stochastic Gradient Clipping on $\mathcal{SO}(n)$ (using Retraction)

```

1:  $m_t \leftarrow 0$ ; ▷ Initialize
2: for  $t = 1, \dots, T$  do
3:    $m_{t+1} \leftarrow \beta_1 m_t + (1 - \beta_1) \mathcal{G}_t$ ; ▷  $\mathcal{G}$  as euclidean gradient estimate
4:    $\hat{\mathcal{G}} \leftarrow \text{Clip}(\tau_{t+1}, m_{t+1})$ ; ▷ Clipping using 18
5:    $m_{t+1} \leftarrow \text{Proj}(\hat{\mathcal{G}})$  ▷ Project onto the tangent space using 14
6:    $x_{t+1} \leftarrow \mathcal{R}_{x_t}(-\eta_t m_{t+1})$  ▷ Retraction,  $\eta_t$  is the learning rate
7: end for
    
```

Coordinate-wise Clipping procedure can be written as follow in two versions of fixed and adaptive in N -coordinates

$$\begin{aligned}
 \text{CCLIP}(\tau_t, m_t) &= \min\left\{\frac{\tau_t}{|m_t|}, 1\right\} m_t, \tau_t \in \mathbb{R}^N \geq 0 \quad \text{or} \\
 \text{ACCLIP}(\tau_t, m_t) &= \min\left\{\frac{\tau_t}{|m_t| + \epsilon}, 1\right\} m_t, \tau_t^\alpha = \beta_2 \tau_{t-1}^\alpha + (1 - \beta_2) |\mathcal{G}_t|^\alpha
 \end{aligned} \quad (18)$$

4 Experiments

This section discusses the experiment's setup and results, including the method proposed in section 3 and a Riemannian adaption of ADAM with a similar approach. Also, as mentioned in section 2, there is a gap in comparison of mentioned methods with a gradient-based unconstrained method; therefore, ADAM and ACCLIP SGD is considered. Furthermore, the factorization mentioned in equation 12 has been combined with unconstrained methods to evaluate its efficiency to reduce the determinant computation. Since the hybrid algorithm of CD-FNMRES EM has shown to have a fast and trustworthy convergence in a large number of components scheme, which outperforms the generalized EM, the ground truth of our comparison would be CD-FNMRES EM with 27 steps of the Coordinate Descents algorithm to run and 73 steps of Fast Newton method. The total number of iterations in the EM-based algorithm is 100, so the number of epochs of stochastic algorithms is the same. The step size (learning rate) in stochastic algorithms is determined by a cosine annealing procedure [32] with a warmup.

In general, two types of experiment has been evaluated: synthetic and real datasets. In all tests, 80% of data has been used for training and the rest for the test. In addition, all datasets have been whitened before entering any procedure. The same initialization was applied in all, and for real datasets with high dimensions, standard PCA has been deployed to reduce the dimensions to not more than 101 with the condition of preserving at least 94% explained variance.

It is worth mentioning, Since the CD-FNMRES EM implementation is on MATLAB[12], and our online method has been implemented with Pytorch, the computation power in all tests has been limited to just a single core of CPU.

4.1 Synthetic Data

First, we need to compare the efficacy of various approaches at recovering genuine underlying distribution parameters. We achieve this by drawing samples from GMMs whose means and covariance matrices are already known. As the separation of the components plays a crucial role in the learning procedure[33], data is generated using technique [16]; therefore, with the following inequality, the separation would be under control using c parameter.

$$\forall_{i \neq j} \|\mu_i - \mu_j\| \geq c \max_{i,j} \{tr(\Sigma_i), tr(\Sigma_j)\}$$

The separation control variable c is set to three thresholds 0.1, 1, and 5, which respectively resemble low, medium, and high separation. All of the synthesized datasets include five components(K) and generated in five-dimensional space(d). Another aspect of performance can be presented in how many data points are needed to achieve convergence; to this end, datasets have been produced in three different sizes; $10d^2$, $100d^2$, and $1000d^2$. In addition, The covariance matrices have an eccentricity of $e = 10$, defined as the ratio of the largest to the smallest eigenvalue, and the batch size for stochastic methods is set to be fixed at 16.

There are three main error indices for evaluation, the Averaged Negative LogLikelihood over ten different datasets -in figures named *Test NLL*, the Summation of Frobenius norms of difference between the Estimated Covariance Matrix and Nominal Covariance Matrix over all components -in figures named *Cov Error*, and the Summation of Cosine similarity distance of difference between the Estimated Mean Vector and Nominal Mean Vector over all components-in figures named *Mean Error*.

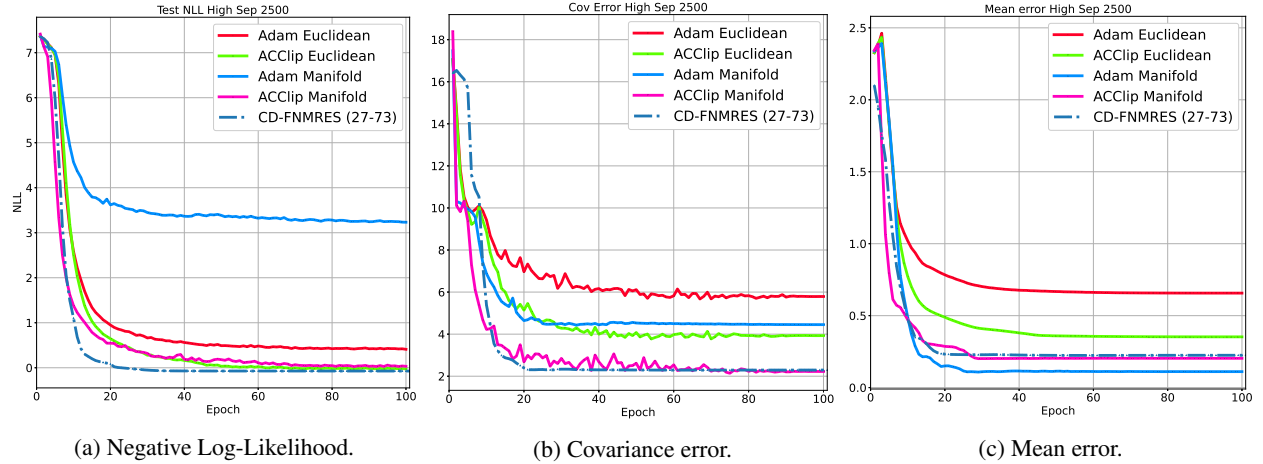


Figure 2: Random Synthetic Data with High Separation with 2500 data points.

4.1.1 Random Data

The random data has no constraints on the shape or volume and were generated with the full covariance matrix assumption. The complete detailed plots can be found in the appendix while a sample is illustrated in Figure2; in general, online methods compete with the ground truth batch method. The same pattern illustrates that with large and medium dataset sizes in all separation categories, the NLL could reach the ground truth or even improve it. However, by reducing the batch size (even going full stochastic with a batch size of one), the results for datasets with medium and small sizes can be improved. The new manifold optimization method outperforms the ADAM version almost in all cases, and in contrast to previous works, it could achieve the best performance over other online methods.

The covariance errors also emphasize the fact that in case of acceptable convergence, a faster decrease in error can be reached by the online methods. On the other hand, the mean vector errors occur to converge more pleasing only in cases with high separation or a large number of data points.

4.1.2 Orthogonal Data

To investigate more about the orthogonality assumption on the covariance matrix via the Felexiby-Tied factorization in equation3, we conduct an experiment the same as the previous section with the shape of the covariance matrix. The covariance matrices have the same structure as UD_kU^T with orthogonal U ; hence the eccentricity factor can be defined on the diagonal elements of matrix D_k . The complete detailed plots can be found in the appendix section

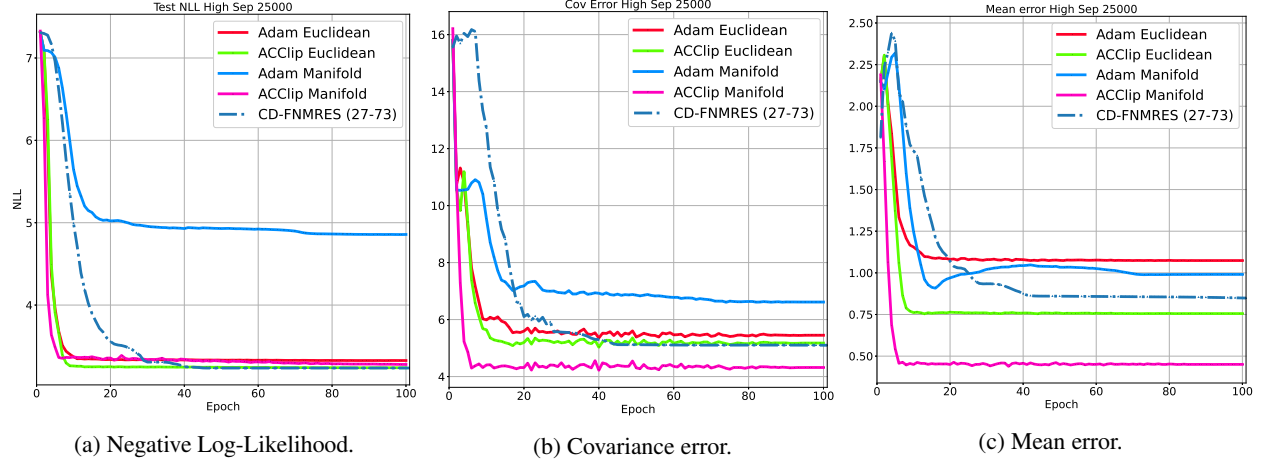


Figure 3: Orthogonal Synthetic Data with High Separation with 25000 data points.

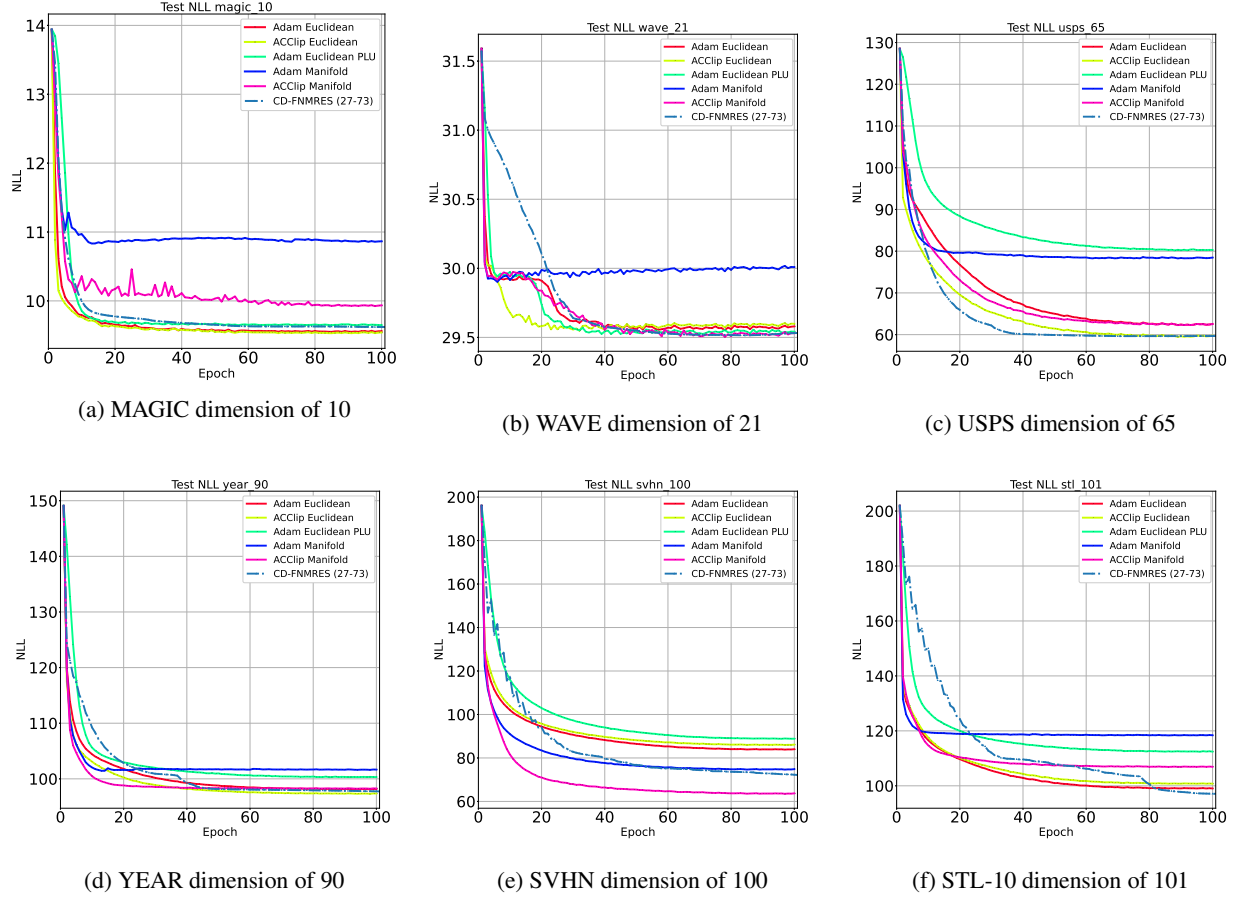


Figure 4: The Test NLL for Real dataset.

while like before a sample is illustrated in Figure3.

In all the cases, the online methods are the faster estimators in the sense that they require fewer epochs for convergence. Also, they gain a competitive or better convergence of NLL except in the circumstance of the high separation with a small dataset. The Em-based algorithm appears to proceed dramatically slow in the first part, which uses coordinate descent due to the orthogonality constraint. The covariance error demonstrates the excellence of the new manifold optimization algorithm, although the decrease in the size of data sets affects the performance of all online methods.

Table 2: the performance characteristics of learning methods

Dataset [Dimension]	Method	Best NLL	Time per Epoch	Comments
MAGIC [10]	Adam Euclidean	9.56	$0.88 \pm 0.02s$	
	ACClip Euclidean	9.54	$1.05 \pm 0.03s$	
	Adam Euclidean PLU	9.64	$1.13 \pm 0.05s$	
	Adam Manifold	10.85	$0.85 \pm 0.03s$	qr Ret
	ACClip Manifold (proposed)	9.93	$1.03 \pm 0.03s$	qr Ret
	CD-FNMRES	9.62	$0.15 \pm 0.03s$	27-73
WAVE [21]	Adam Euclidean	29.57	$0.49 \pm 0.01s$	
	ACClip Euclidean	29.58	$0.57 \pm 0.01s$	
	Adam Euclidean PLU	29.54	$0.72 \pm 0.04s$	
	Adam Manifold	29.99	$0.43 \pm 0.01s$	qr Ret
	ACClip Manifold (proposed)	29.51	$0.65 \pm 0.02s$	qr Ret
	CD-FNMRES	29.53	$0.23 \pm 0.03s$	27-73
USPS [65]	Adam Euclidean	62.51	$4.43 \pm 0.44s$	
	ACClip Euclidean	59.63	$4.75 \pm 0.37s$	
	Adam Euclidean PLU	80.24	$8.95 \pm 0.94s$	
	Adam Manifold	78.47	$3.77 \pm 0.40s$	qr Ret
	ACClip Manifold (proposed)	62.52	$4.62 \pm 0.37s$	qr Ret
	CD-FNMRES	59.66	$15.75 \pm 8.37s$	27-73
YEAR [90]	Adam Euclidean	98.16	$94.63 \pm 5.53s$	
	ACClip Euclidean	97.31	$103.34 \pm 5.87s$	
	Adam Euclidean PLU	100.31	$195.47 \pm 16.31s$	
	Adam Manifold	101.61	$78.13 \pm 4.07s$	qr Ret
	ACClip Manifold (proposed)	98.22	$97.37 \pm 3.72s$	qr Ret
	CD-FNMRES	97.74	$141.06 \pm 60.20s$	27-73
SVHN [100]	Adam Euclidean	83.90	$83.37 \pm 6.49s$	
	ACClip Euclidean	85.95	$90.41 \pm 6.54s$	
	Adam Euclidean PLU	88.82	$185.96 \pm 19.33s$	
	Adam Manifold	74.64	$86.04 \pm 3.19s$	qr Ret
	ACClip Manifold (proposed)	63.57	$85.01 \pm 6.27s$	qr Ret
	CD-FNMRES	72.17	$216.30 \pm 107.42s$	27-73
STL [101]	Adam Euclidean	99.04	$106.47 \pm 6.02s$	
	ACClip Euclidean	100.76	$111.63 \pm 6.71s$	
	Adam Euclidean PLU	112.43	$248.16 \pm 24.83s$	
	Adam Manifold	118.40	$110.35 \pm 7.19s$	qr Ret
	ACClip Manifold (proposed)	106.90	$106.44 \pm 9.02s$	qr Ret
	CD-FNMRES	97.08	$254.04 \pm 120.49s$	27-73

4.2 Real Data

For the last setup of experiments, we conduct a fair procedure(in sense of computation power allocation and initialization) to evaluate the online methods(including ours) and compare them with the EM-based method over real data with a large number of components.

Since the GMM has been known not to be desirable with image data and computer vision tasks, we include image datasets for our experiments. The datasets used in this section are: "Magic Gamma Telescope"[34], "Wave Energy Converters"[35], "SVHN "[36], "STL-10 "[37], "USPS"[38], and "YearPredictionMSD" available via <https://archive.ics.uci.edu/ml/datasets>. To lift the structural variable (Hyperparameter of GMMs) obli-

gation, the number of Gaussian components in each example is the same as the dimension of the dataset itself.

The results of Figure 4 and Table 2 portray this fact, at least one of the online algorithms fulfills a better convergence than the EM-based algorithm. Except for the STL-10 dataset, in which the EM-based method is inferior to the online method till the last 20 epochs, the conjugate gradient method could escape the local minimum because of its property. Also, in all cases, the proposed ACCLipping SGD on manifold is superior to the ADAM version and outperforms others on the SVHN dataset.

Furthermore, in all examples, the best online method converges to an optimal point with fewer epochs, excluding the USPS dataset. Moreover, The time consumption per epoch/iteration becomes in favor of online methods by increasing the dimension (up to four times as fast). Besides the PLU factorization, which consumes more time per each epoch with the increase of the dimension.

Please note in Table 2, the time consumption of manifold adaption of ADAM is not marked due to unacceptable convergence, and the closest rival with better convergence is chosen.

5 Conclusions

In this paper, we proposed a framework for online learning of GMMs by using the first-order stochastic methods for GMMs in high-dimensional space and a large number of components. Flexibly-Tied factorization of covariance matrices is used to achieve this goal, which constructs a differentiable maximum likelihood problem. The orthogonality constraint arises along the parameter-sharing scheme. A new stochastic manifold optimizer (Coordinate-wise Clipping SGD on $\mathcal{SO}(n)$) is proposed to handle the orthogonality constraint. The empirical experiments verify that the online regime converges faster (in the sense of the number of epochs), with less computation time in high dimensions, and outperforms the EM-based method in many cases. The proposed framework can be used in various domains that need an online estimation of Large-Scale GMM due to the simplicity of implementation. Moreover, the proposed method enables cascading the popular deep neural network models to a powerful kernel model with an end-to-end learning procedure.

Furthermore, the stochastic manifold optimizer illustrates that despite the previous assumptions, orthogonality may not restrict the model to low-dimensional space, and with even better time performances than its Euclidean counterpart, it can be used in more complex models such as deep neural networks to preserve orthogonality during the training phase. At last, the PLU factorization has empirically shown acceptable neither convergence nor time performance.

References

- [1] Geoffrey J McLachlan, Sharon X Lee, and Suren I Rathnayake. Finite mixture models. *Annual review of statistics and its application*, 6:355–378, 2019.
- [2] Jacob Goldberger, Shiri Gordon, Hayit Greenspan, et al. An efficient image similarity measure based on approximations of kl-divergence between two gaussian mixtures. In *ICCV*, volume 3, pages 487–493, 2003.
- [3] S Mohammad Khansari-Zadeh and Aude Billard. Learning stable nonlinear dynamical systems with gaussian mixture models. *IEEE Transactions on Robotics*, 27(5):943–957, 2011.
- [4] Mahdi M Kalayeh and Mubarak Shah. Training faster by separating modes of variation in batch-normalized models. *IEEE transactions on pattern analysis and machine intelligence*, 42(6):1483–1500, 2019.
- [5] Soheil Kolouri, Gustavo K Rohde, and Heiko Hoffmann. Sliced wasserstein distance for learning gaussian mixture models. In *Proceedings of the IEEE Conference on Computer Vision and Pattern Recognition*, pages 3427–3436, 2018.
- [6] Eitan Richardson and Yair Weiss. On gans and gmms. *Advances in Neural Information Processing Systems*, 31, 2018.
- [7] Arthur P Dempster, Nan M Laird, and Donald B Rubin. Maximum likelihood from incomplete data via the em algorithm. *Journal of the Royal Statistical Society: Series B (Methodological)*, 39(1):1–22, 1977.
- [8] Christopher M Bishop. Mixture density networks. 1994.
- [9] Richard A Redner and Homer F Walker. Mixture densities, maximum likelihood and the em algorithm. *SIAM review*, 26(2):195–239, 1984.
- [10] Geoffrey J McLachlan and Thiriyambakam Krishnan. *The EM algorithm and extensions*. John Wiley & Sons, 2007.
- [11] Radford M Neal and Geoffrey E Hinton. A view of the em algorithm that justifies incremental, sparse, and other variants. In *Learning in graphical models*, pages 355–368. Springer, 1998.

- [12] Hadi Asheri, Reshad Hosseini, and Babak Nadjar Araabi. A new em algorithm for flexibly tied gmms with large number of components. *Pattern Recognition*, 114:107836, 2021.
- [13] Chi Jin, Yuchen Zhang, Sivaraman Balakrishnan, Martin J Wainwright, and Michael I Jordan. Local maxima in the likelihood of gaussian mixture models: Structural results and algorithmic consequences. *Advances in neural information processing systems*, 29, 2016.
- [14] Robert J Vanderbei and H Yurttan Benson. On formulating semidefinite programming problems as smooth convex nonlinear optimization problems. *Technical Report*, 2000.
- [15] Reshad Hosseini and Suvrit Sra. Matrix manifold optimization for gaussian mixtures. *Advances in Neural Information Processing Systems*, 28:910–918, 2015.
- [16] Reshad Hosseini and Suvrit Sra. An alternative to em for gaussian mixture models: batch and stochastic riemannian optimization. *Mathematical Programming*, 181(1):187–223, 2020.
- [17] Shun-Ichi Amari. Natural gradient works efficiently in learning. *Neural computation*, 10(2):251–276, 1998.
- [18] Mark JF Gales. Semi-tied covariance matrices for hidden markov models. *IEEE transactions on speech and audio processing*, 7(3):272–281, 1999.
- [19] Chris Fraley and Adrian E Raftery. Bayesian regularization for normal mixture estimation and model-based clustering. *Journal of classification*, 24(2):155–181, 2007.
- [20] Andrea Ridolfi and Jérôme Idier. Penalized maximum likelihood estimation for univariate normal mixture distributions. In *AIP Conference Proceedings*, volume 568, pages 229–237. American Institute of Physics, 2001.
- [21] Christophe Biernacki, Gilles Celeux, Gérard Govaert, and Florent Langrognet. Model-based cluster and discriminant analysis with the mixmod software. *Computational Statistics & Data Analysis*, 51(2):587–600, 2006.
- [22] Durk P Kingma and Prafulla Dhariwal. Glow: Generative flow with invertible 1x1 convolutions. *Advances in neural information processing systems*, 31, 2018.
- [23] Ruslan Salakhutdinov, Sam T Roweis, and Zoubin Ghahramani. Optimization with em and expectation-conjugate-gradient. In *Proceedings of the 20th International Conference on Machine Learning (ICML-03)*, pages 672–679, 2003.
- [24] Gilles Celeux and Gérard Govaert. Gaussian parsimonious clustering models. *Pattern recognition*, 28(5):781–793, 1995.
- [25] Michael I Jordan and Robert A Jacobs. Hierarchical mixtures of experts and the em algorithm. *Neural computation*, 6(2):181–214, 1994.
- [26] Diederik P Kingma and Jimmy Ba. Adam: A method for stochastic optimization. *arXiv preprint arXiv:1412.6980*, 2014.
- [27] Jingzhao Zhang, Sai Praneeth Karimireddy, Andreas Veit, Seungyeon Kim, Sashank J Reddi, Sanjiv Kumar, and Suvrit Sra. Why adam beats sgd for attention models. 2019.
- [28] P-A Absil, Robert Mahony, and Rodolphe Sepulchre. Optimization algorithms on matrix manifolds. In *Optimization Algorithms on Matrix Manifolds*. Princeton University Press, 2009.
- [29] Nicolas Boumal. An introduction to optimization on smooth manifolds. *Available online*, May, 3, 2020.
- [30] Jun Li, Li Fuxin, and Sinisa Todorovic. Efficient riemannian optimization on the stiefel manifold via the cayley transform. *arXiv preprint arXiv:2002.01113*, 2020.
- [31] Silvere Bonnabel. Stochastic gradient descent on riemannian manifolds. *IEEE Transactions on Automatic Control*, 58(9):2217–2229, 2013.
- [32] Ilya Loshchilov and Frank Hutter. Sgdr: Stochastic gradient descent with warm restarts. *arXiv preprint arXiv:1608.03983*, 2016.
- [33] Lei Xu and Michael I Jordan. On convergence properties of the em algorithm for gaussian mixtures. *Neural computation*, 8(1):129–151, 1996.
- [34] RK Bock, A Chilingarian, M Gaug, F Haki, Th Hengstebeck, M Jiřina, J Klaschka, E Kotrč, P Savický, S Towers, et al. Methods for multidimensional event classification: a case study using images from a cherenkov gamma-ray telescope. *Nuclear Instruments and Methods in Physics Research Section A: Accelerators, Spectrometers, Detectors and Associated Equipment*, 516(2-3):511–528, 2004.
- [35] LD Mann, AR Burns, and ME Ottaviano. Ceto, a carbon free wave power energy provider of the future. In *Proceedings of the 7th European Wave and Tidal Energy Conference (EWTEC)*, volume 108, 2007.

- [36] Yuval Netzer, Tao Wang, Adam Coates, Alessandro Bissacco, Bo Wu, and Andrew Y Ng. Reading digits in natural images with unsupervised feature learning. 2011.
- [37] Adam Coates, Andrew Ng, and Honglak Lee. An analysis of single-layer networks in unsupervised feature learning. In *Proceedings of the fourteenth international conference on artificial intelligence and statistics*, pages 215–223. JMLR Workshop and Conference Proceedings, 2011.
- [38] Jonathan J. Hull. A database for handwritten text recognition research. *IEEE Transactions on pattern analysis and machine intelligence*, 16(5):550–554, 1994.

Appendix

Synthetic Data

In this section, we provide the result of synthetic data experiments from section 4.1. The figures 5-13 refer to the results of random simulated data(section4.1.1), and The figures 14-22 refer to the results of orthogonal simulated data(section4.1.2).

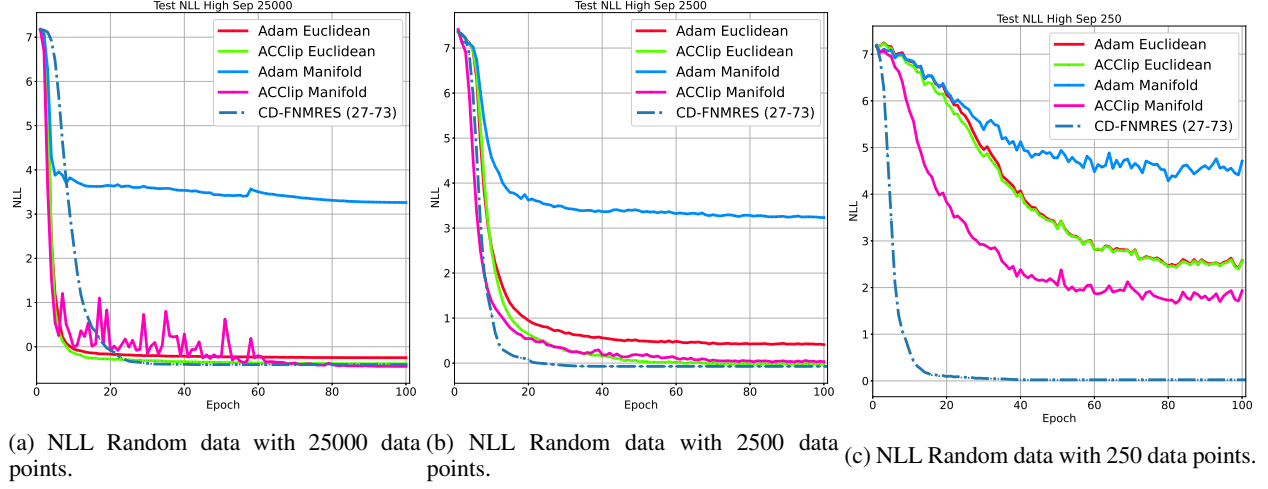


Figure 5: NLL of Random Synthetic Data with High Separation.

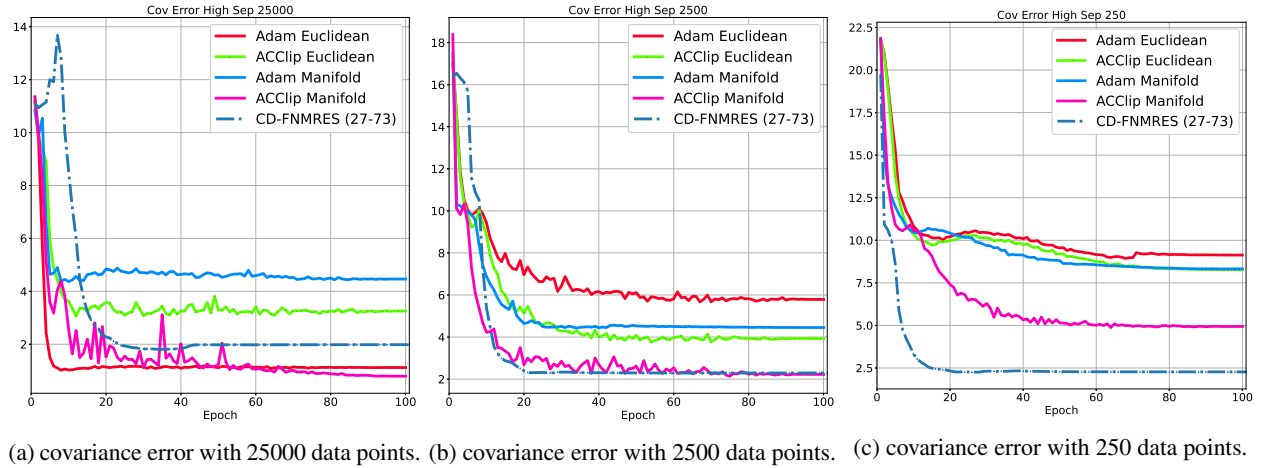


Figure 6: Covariance Estimation Error of Random Synthetic Data with High Separation.

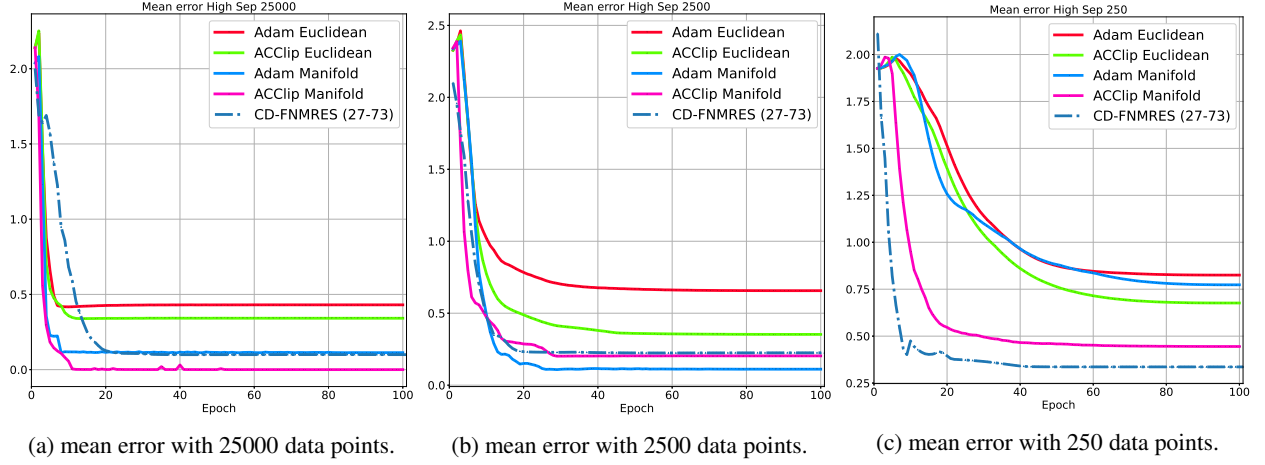


Figure 7: Mean Vector Estimation Error of Random Synthetic Data with High Separation.

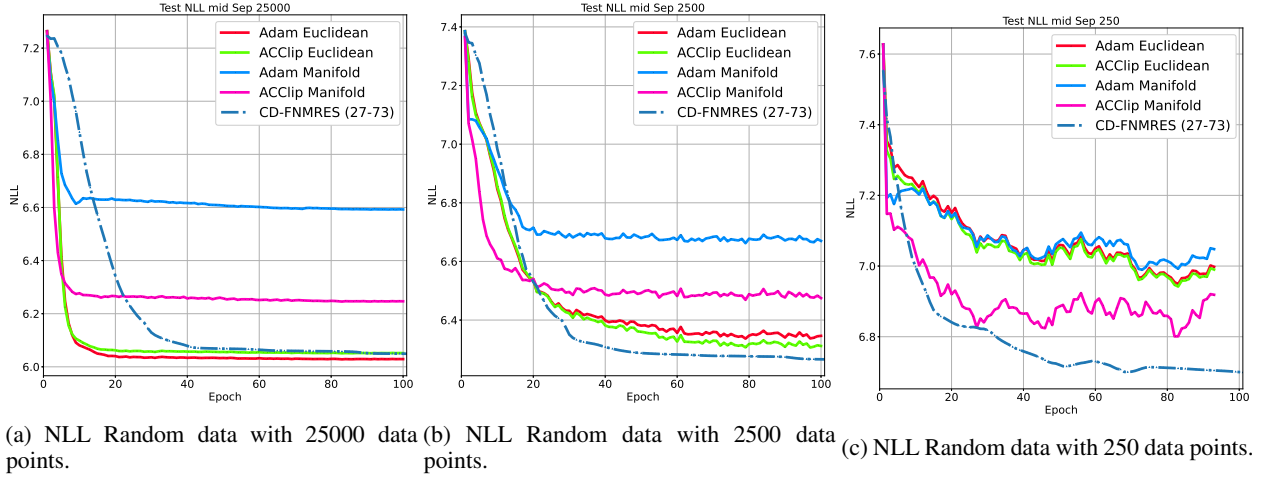


Figure 8: NLL of Random Synthetic Data with Mid Separation.

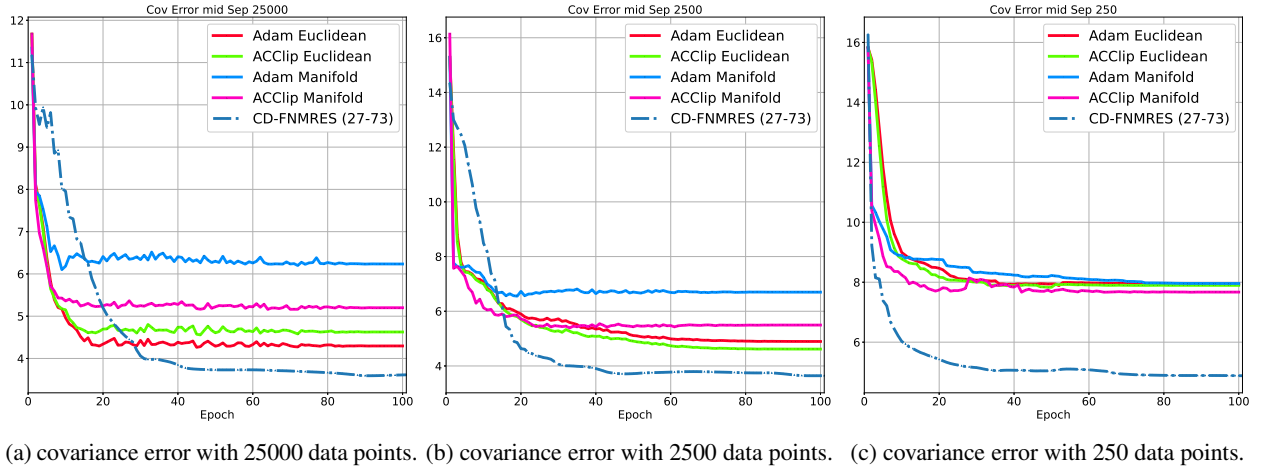


Figure 9: Covariance Estimation Error of Random Synthetic Data with Mid Separation.

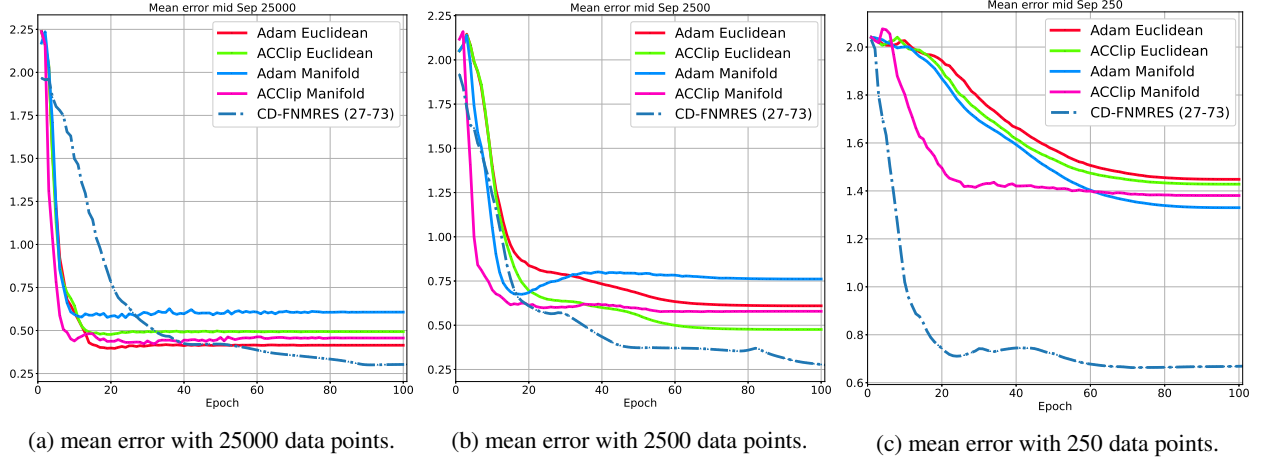


Figure 10: Mean Vector Estimation Error of Random Synthetic Data with Mid Separation.

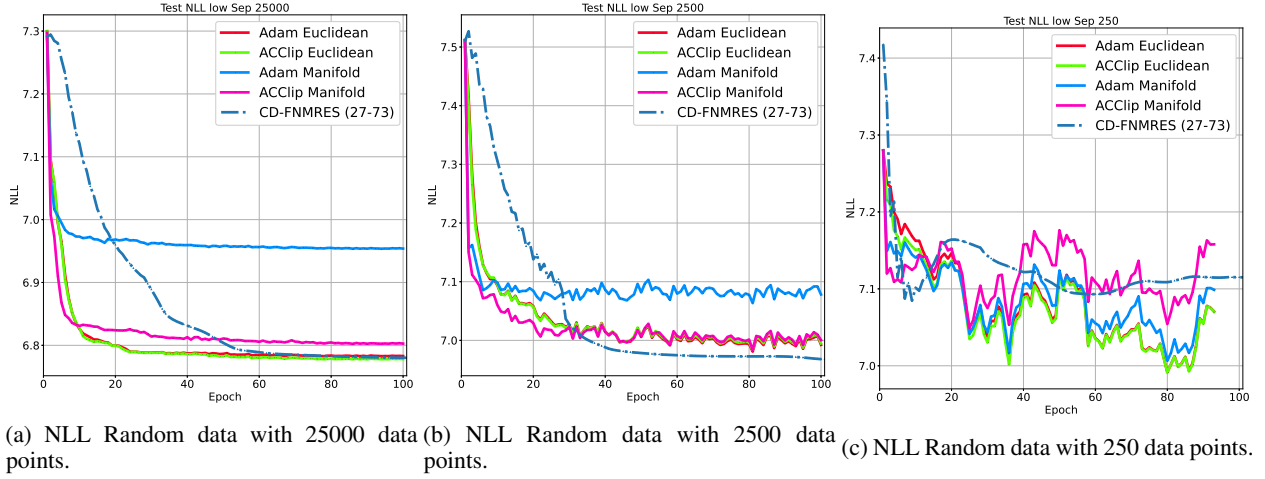


Figure 11: NLL of Random Synthetic Data with Low Separation.

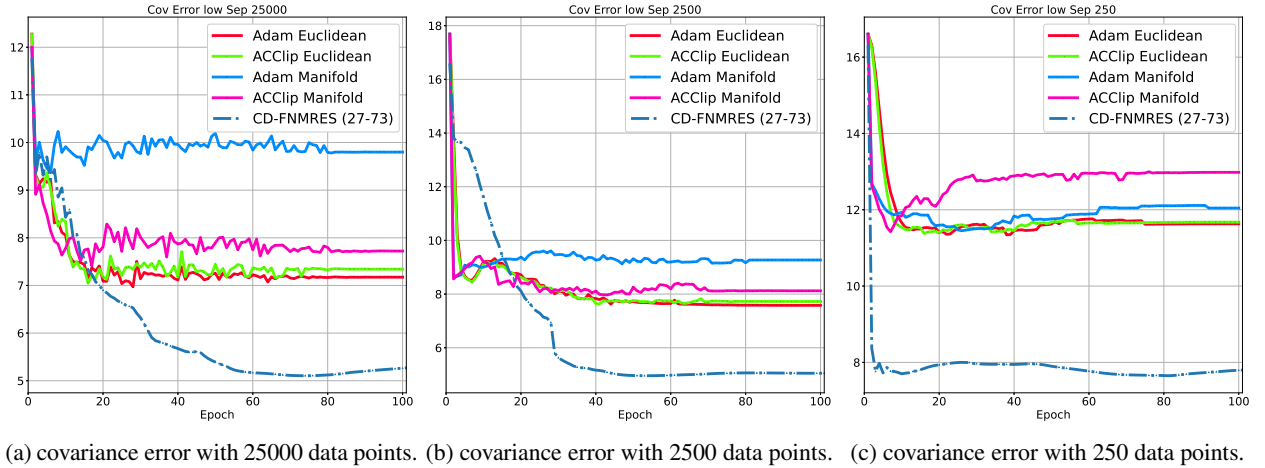


Figure 12: Covariance Estimation Error of Random Synthetic Data with Low Separation.

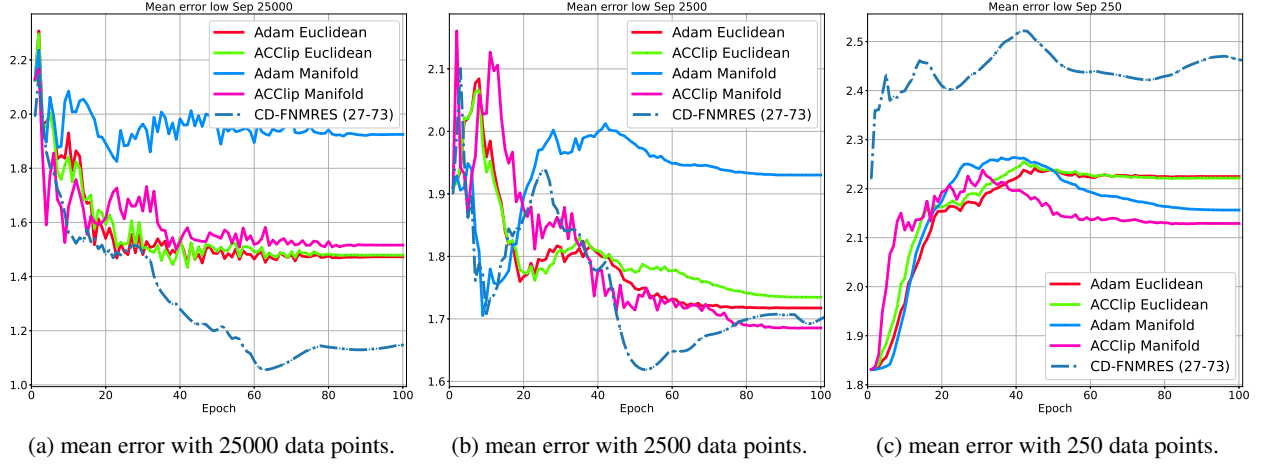


Figure 13: Mean Vector Estimation Error of Random Synthetic Data with Low Separation.

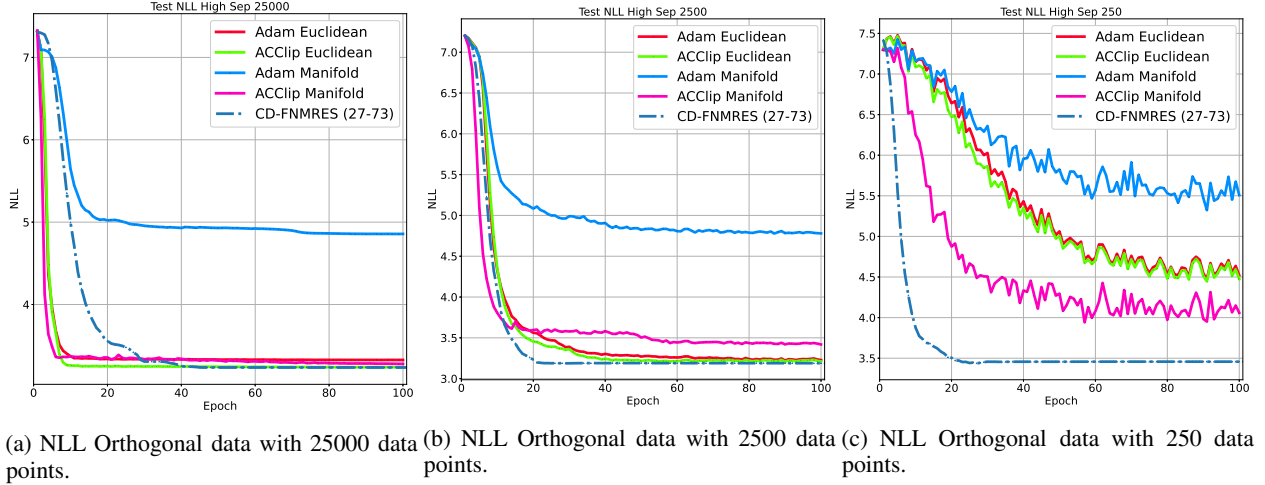


Figure 14: NLL of Orthogonal Synthetic Data with High Separation.

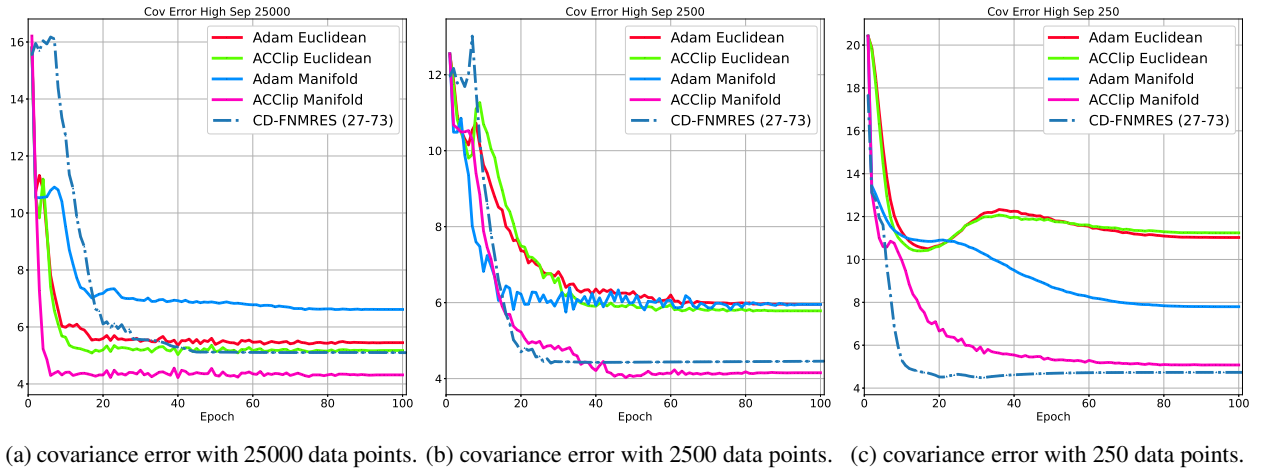


Figure 15: Covariance Estimation Error of Orthogonal Synthetic Data with High Separation.

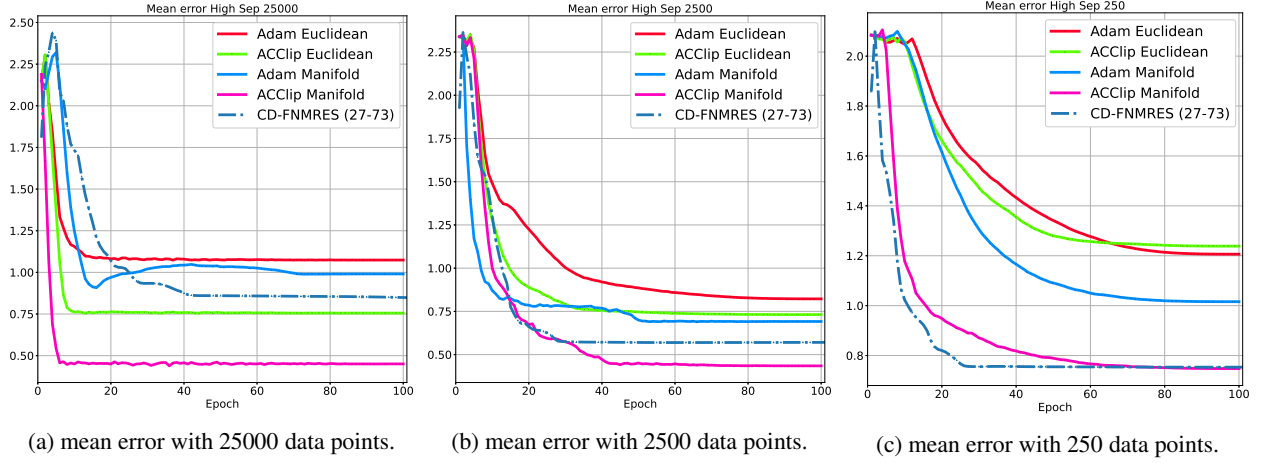


Figure 16: Mean Vector Estimation Error of Orthogonal Synthetic Data with High Separation.

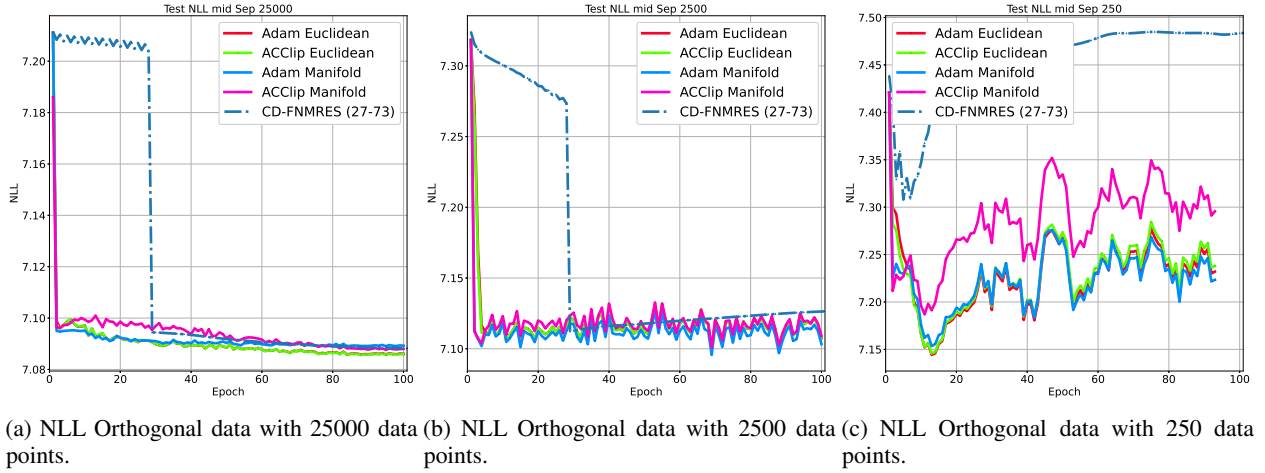


Figure 17: NLL of Orthogonal Synthetic Data with Mid Separation.

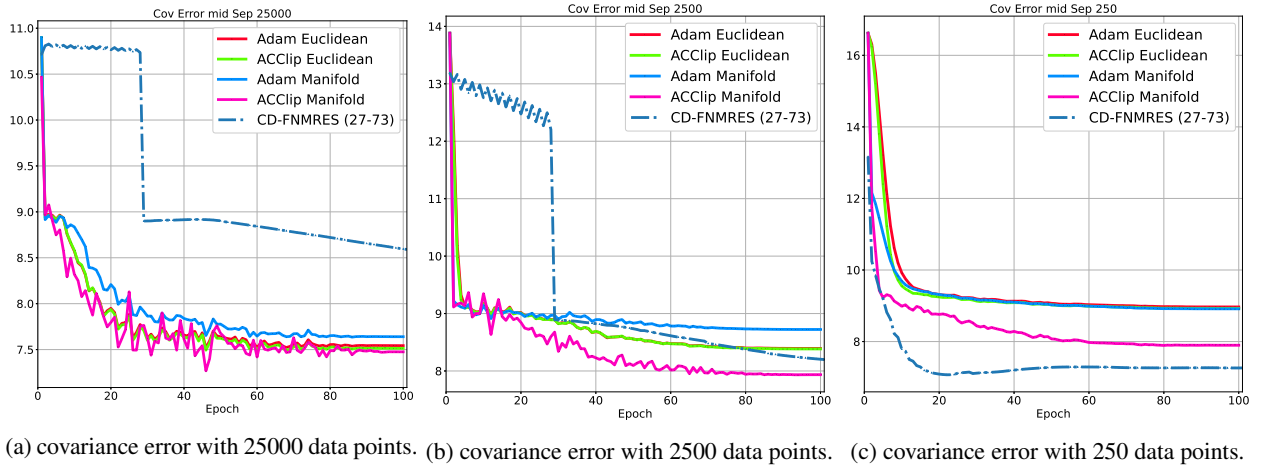


Figure 18: Covariance Estimation Error of Orthogonal Synthetic Data with Mid Separation.

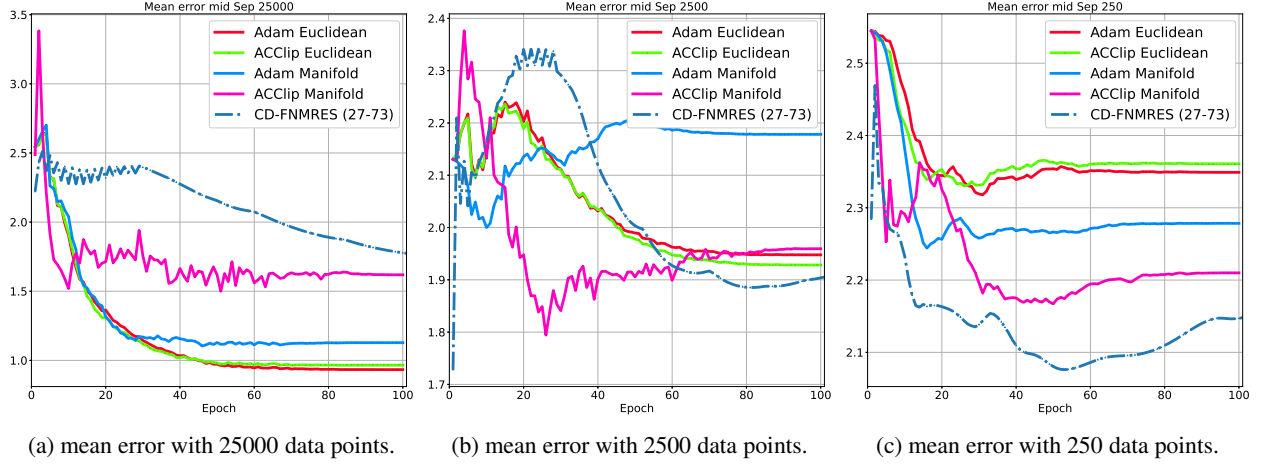


Figure 19: Mean Vector Estimation Error of Orthogonal Synthetic Data with Mid Separation.

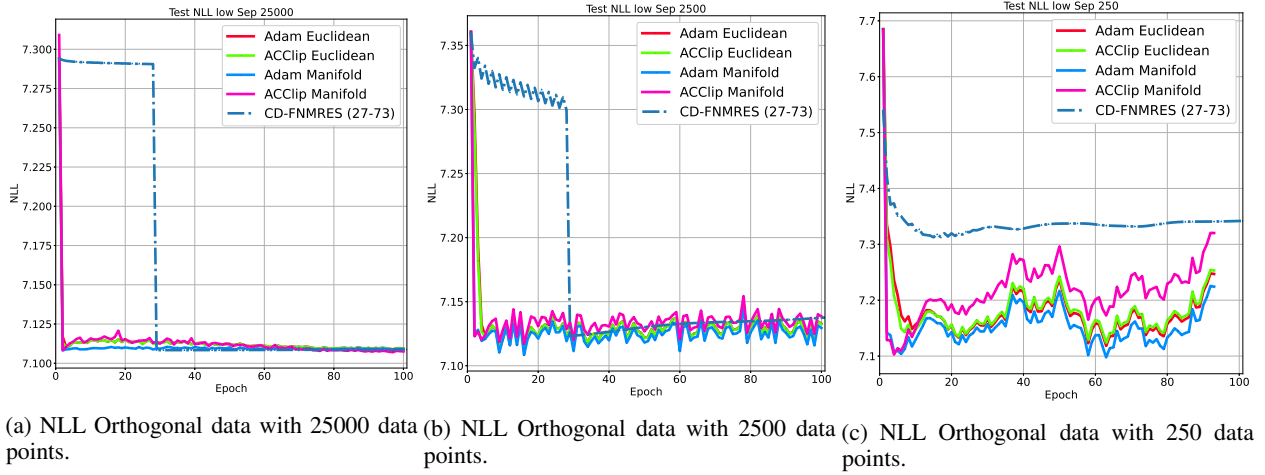


Figure 20: NLL of Orthogonal Synthetic Data with Low Separation.

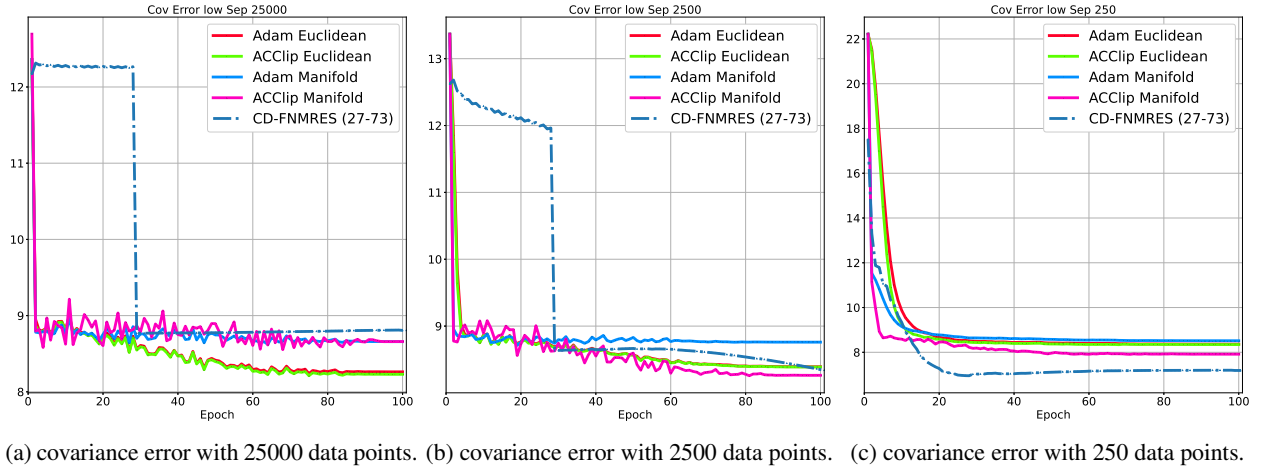


Figure 21: Covariance Estimation Error of Orthogonal Synthetic Data with Low Separation.

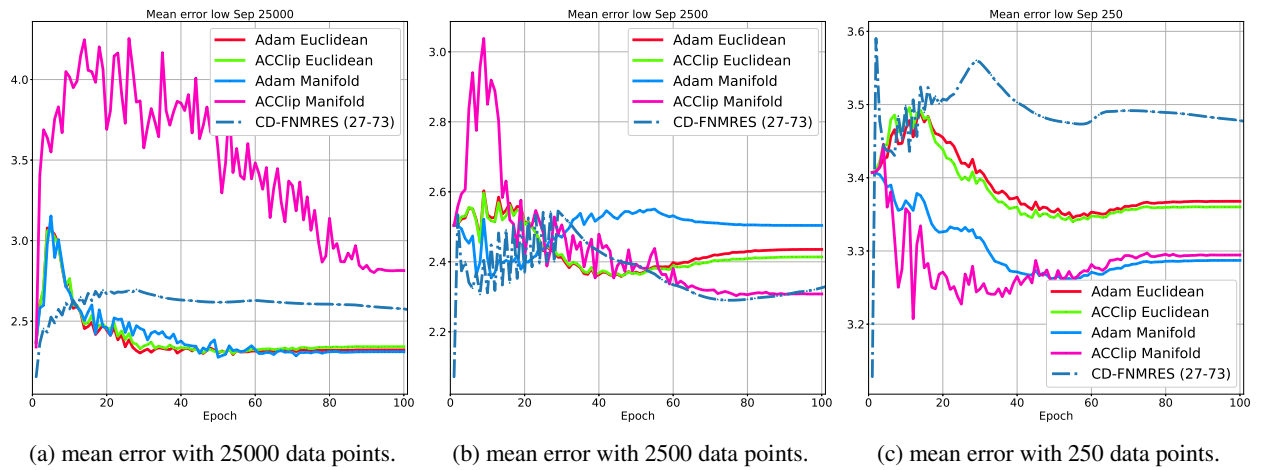


Figure 22: Mean Vector Estimation Error of Orthogonal Synthetic Data with Low Separation.